

Thermodynamic instability in supersaturated lysozyme solutions: Effect of salt and role of concentration fluctuations

Mauro Manno,^{1,*} Caide Xiao,² Donatella Bulone,¹ Vincenzo Martorana,¹ and Pier Luigi San Biagio¹
¹National Research Council Italy, Institute of Biophysics (Palermo), Via Ugo La Malfa 153, 90146 Palermo, Italy
²Biotechnology Research Institute, National Research Council Canada, Montreal, Quebec, Canada H4P2R2

(Received 4 April 2003; published 14 July 2003)

Experimental and theoretical work has suggested that protein crystal nucleation can be affected by the separation of two metastable liquid phases with different local concentrations, or more specifically by critical density fluctuations. We measure the amplitude and correlation length of local concentration fluctuations by light scattering for supersaturated solutions of hen egg-white lysozyme (at pH 4.5 and at different NaCl concentrations, up to 7% w/v). By extrapolating the critical divergent behavior of concentration fluctuation amplitude versus temperature, we determine the spinodal line, that is the limit of stability. Cloud-point measurements are used to determine liquid-liquid coexistence, consistent with previous work. In the present work, which is an extensive study of off-critical fluctuations in supersaturated protein solution, we observe a non-classical scaling divergent behavior of the correlation length of concentration fluctuations, thus suggesting that off-critical fluctuations may have a role in crystallization kinetics. To appropriately fit the spinodal data, an entropic term must be added to the van der Waals or to the adhesive hard-sphere model. We interpret this contribution as due to the salt-induced modulation of protein hydration.

DOI: 10.1103/PhysRevE.68.011904

PACS number(s): 87.15.Nn, 64.70.Ja, 87.15.Ya, 64.10.+h

I. INTRODUCTION

Mechanisms that control protein association and nucleation are important to many fields such as pathological protein deposition in neurodegenerative diseases [1], industrial separation processes by salt-induced precipitation, protein crystallization [2], or protein gelation (relevant, e.g., in the food industry). However, the interactions leading to protein aggregation or crystallization, and eventual precipitation, are not clearly understood. For instance, protein crystallization, which is a major bottleneck in determining protein three-dimensional structure, is still achieved by semiempirical (time-consuming) methods, often depending on the crystallographer's skills.

An experimental route to the study of protein interactions includes the determination of phase diagrams and the study of phase transitions which drive a metastable protein solution towards the stable equilibrium state in which large aggregates, crystals, or precipitates coexist with the solution. The ordering transition from the homogeneous solution to the equilibrium coexistence of solid and liquid phases can involve other metastable intermediate states. Indeed, phase diagrams of some proteins exhibit a liquid-liquid coexistence region, that is, a range of temperatures and concentrations in which two liquid phases with different local concentrations can be formed. This was first observed by Ishimoto and Tanaka in lysozyme solutions [3], and subsequently found in other proteins and under different conditions [4–14]. In some cases (lysozyme, γ -crystallin), liquid-liquid coexistence is metastable with respect to crystallization [3–12].

Metastability of liquid-liquid coexistence has been clarified by work on colloids [15–17]. Such studies have pointed out that the range of attraction between colloids in solution may be the basic parameter in the determination of the phase diagram. Further theoretical studies have shown that by reducing the range of the attraction potential, the liquid-liquid phase transition becomes more and more hindered by the solid-liquid coexistence line [18–21]. Indeed, proteins typically crystallize under condition where electrostatic interactions are screened by salt cosolutes.

Crystallization conditions for many proteins lie in a narrow range of values of the second virial coefficient (crystallization slot) [22]. An interpretation of the crystallization slot based on the (short-range) adhesive hard-spheres model, has pointed out that crystallization may be enhanced close to the critical point of a liquid-liquid phase transition [19]. In general, liquid-liquid metastable phase transitions affect the kinetics of protein association [23] by altering crystal nucleation rates in the region of liquid-liquid stability [24–27] or by preceding crystallization with nucleation or spinodal demixing [28–31].

However, many other questions remain open. For example, the effect of high ionic strength (required for crystallization) cannot be explained in the framework of classical DLVO theory [32,33]. Also, simulations and theoretical studies have shown that critical concentration fluctuations near the critical point may reduce the free-energy barrier for crystal nucleation [34–36], but the role of off-critical fluctuations is not clear. Liquid-liquid phase transitions have been suggested to have an analogous role in the aggregation or gelation of protein solutions [13,14,37].

In the present work, we initiate a study of the liquid-liquid instability curve and the behavior of fluctuations in supersaturated lysozyme solutions at various NaCl concentrations. Knowledge of the complete phase diagram at different salt

*Electronic addresses: mauro@iaif.pa.cnr.it,
mauro.manno@pa.ibf.cnr.it

concentrations should provide a clue for understanding the interactions involved. Further, concentration fluctuations should grow close to the liquid-liquid instability curve (spinodal curve), as well as to the critical point [38,39]. Thus, an extensive characterization of their behavior near the liquid-liquid instability can shed light on the role of fluctuations in the overall crystallization process.

We have performed static and dynamic light scattering experiments at several protein and salt concentrations. We started from the same experimental conditions set in the work of Mushol and Rosenberger [11], who show the most complete phase diagram for three NaCl concentrations, by measuring both the liquid-liquid (cloud-points) and the solid-liquid (solubility) coexistence curves. We found that both the amplitude and correlation length of concentration fluctuations diverge as the temperature is lowered from above the cloud-point temperature. By extrapolating the scaling behavior of this divergence we determined the spinodal temperature for each concentration.

The correlation length of concentration fluctuations was found to exhibit a divergent scaling behavior even in a region not so close to the thermodynamic instability. This suggests that fluctuations could have a critical role in crystallization kinetics also at off-critical concentrations. Interestingly, we find that this divergence is given by a nonclassical exponent $\nu = 0.63 \pm 0.03$, while compressibility diverges with a classical exponent $\gamma = 1.0 \pm 0.01$. This puzzling result is discussed in the paper.

Finally, spinodal lines have been fit by representing protein interactions by two similar models which take into account steric repulsion, short-range attraction, and long-range interactions. The essential role of an entropic contribution due to hydration forces clearly emerges from our analysis and it suggests that salting-out operates via a modulation of such hydration effect (consistently with other results on lysozyme solutions [10,12]).

II. MATERIALS AND METHODS

A. Sample preparation

Lysozyme is a globular protein with an approximately ellipsoidal shape, a molecular mass of 14 400 Dalton (129 residues) and volume $v_p = (\pi/6)45 \times 30 \times 30 \text{ \AA}^3$. Hen egg-white lysozyme (three times crystallized, dialyzed and lyophilized) was purchased from Sigma Chemical Co. and used without further purification. All other chemicals were reagent grade. The buffer solution was 0.1 M sodium acetate and acetic acid in freshly prepared Millipore Super-Q water, at $pH = 4.5$. The pH value was readjusted after dissolution of either 3%, 4%, 5%, or 7% (w/v) NaCl.

Lysozyme solutions were prepared by the following procedure [11]. Protein powder was directly dissolved in buffer solution, gently tapped, and heated in warm water (ca. 45 °C) to expedite protein dissolution and keep the sample well above the temperature of liquid-liquid metastability. Sample was centrifuged at 8000 g for 10 min to remove small amounts of undissolved material and air bubbles, and then directly filtered into a quartz cell through a 0.22 μm Millipore syringe filter.

A small aliquot (50–100 μl) of sample was diluted with buffer solution for UV absorption spectroscopy measurements (Jasco J-530 spectrometer) in order to determine the sample concentration. The extinction coefficient for lysozyme at 280 nm was taken as $\epsilon_{280} = 2.64 \text{ (cm mg/ml)}^{-1}$ [40]. The protein volume fraction ϕ was obtained by multiplying mass concentration c_p by the partial specific volume of lysozyme $v_0 = 0.703 \text{ (ml/g)}$ [40].

B. Experiments

Static and dynamic light scattering experiments were performed at different protein and salt concentrations. Samples were placed in a thermostated cell compartment of a Brookhaven Instruments BI200-SM goniometer. The temperature was controlled within 0.05 °C by using a thermostated recirculating bath. Starting from well above the temperature of liquid-liquid metastability, a downward temperature scanning was performed at a fixed rate between 3 and 5 °C/hour. The scanning rate was chosen as a good compromise between a sufficiently slow rate to allow thermal equilibration of the sample before each measure and a sufficiently fast one to avoid the occurrence of crystal nucleation.

The scattered light intensity, at 90°, and its time autocorrelation function $g_2(t)$ were measured by using a Brookhaven BI-9000 correlator and a 100 mW Ar laser tuned at $\lambda_0 = 514.5 \text{ nm}$. A photodiode positioned at 0° was used to collect forward scattered light and to measure the sample turbidity.

Autocorrelation functions $g_2(t)$ were found to be well fitted by a single exponential function $g_2(t) = 1 + |A \exp(-t/\tau)|^2$, where τ is the correlation (or relaxation) time of a diffusional process, related to single Brownian molecules or to local concentration fluctuations. It can be shown (and it was, in fact, verified for the present case at higher temperatures) that for a diffusional process, $\tau^{-1} = Dq^2$, where D is the apparent diffusion coefficient and q is the scattering vector [which depends upon the scattering angle θ by the relation $q = 4\pi\tilde{n}\lambda_0^{-1} \sin(\theta/2)$, where \tilde{n} is the medium refractive index [41]]. The quality of the single exponential fit and the stability of amplitude A were carefully checked in order to confidently rule out the measurements affected by the occurrence of crystal nucleation or by the formation of larger clusters.

The behavior of the solution viscosity during the temperature scan was checked in one case ($\phi = 0.10, 5\%$ w/v NaCl) by using a stress-controlled AR-1000 rheometer (TA instruments, UK) equipped with a standard-size double concentric aluminum cylinder. As expected, no divergent behavior for viscosity was observed in our temperature range, and thus a constant value equal to the background viscosity of salt-water solutions has been assumed.

III. DETERMINATION OF PHASE DIAGRAMS

A. Liquid-liquid coexistence: Cloud points

A typical temperature scanning experiment is shown in Fig. 1. Both the scattered intensity and correlation time in-

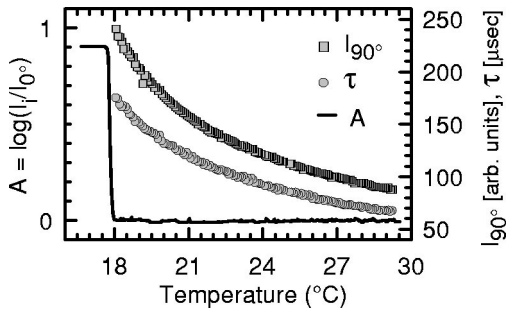


FIG. 1. Typical temperature scanning experiment (NaCl 5% w/v, $\phi = 0.056$). Squares: 90° scattered intensity. Circles: relaxation time τ , as obtained from correlation function. Solid line: turbidity $A = \log_{10}(I_i/I_0)$, where I_i is incident intensity and I_0 is forward scattered intensity.

crease by lowering the temperature, while the turbidity is essentially constant. At a certain temperature, the transmitted intensity suddenly drops to a very low value and the sample becomes turbid or “cloudy” (cloud point). Dynamic and static light scattering measurements are not possible beyond this point due to multiple scattering.

At each given concentration, the cloud-point temperature marks the onset of the liquid-liquid phase separation. Indeed, sample opacity is due to fast formation of domains of higher and lower protein local concentration, which leads to the coexistence of two liquid phases with different local concentrations and equal pressure and chemical potential: $P(\phi_1) = P(\phi_2)$, $\mu(\phi_1) = \mu(\phi_2)$ [42]. These relations define, in the temperature-concentration plane, the so-called binodal line.

Our experimental cloud points are reported in Fig. 2 (together with spinodal points, to be discussed in the following section). They are in full agreement with the results of Mushol and Rosenberger [11] for NaCl concentrations of 3, 5, and 7% w/v. The binodal points for the case of 4% w/v NaCl are reported here for the first time, to the best of our knowledge, and they essentially extend and confirm the previous work.

Within the framework of phase transition theory, the difference between the concentrations of two coexisting phases can be seen as a (nonzero) order parameter [43]. Thus, near the critical point, the binodal line can be described by the following scaling relation:

$$\left| \frac{\phi_c - \phi}{\phi_c} \right| = A \left(\frac{T_c - T}{T_c} \right)^\beta, \quad (1)$$

where T_c and ϕ_c are, respectively, the critical temperature and volume fraction, A is a constant, and β is a critical exponent.

In Fig. 2 we have reported the binodal lines as described by Eq. (1), with $\beta = 0.325$, $\phi_c = 0.177$ and $T_c = 32.5, 22.5, 15.0$, and 8.1°C , respectively, for [NaCl] = 7%, 5%, 4%, 3% w/v. This value of the critical exponent β is consistent with that obtained by renormalization-group calculations, while mean-field theory would predict $\beta = 0.5$ [44]. A nonclassical value for β has been found in analogous experiments on lysozyme or other proteins [5,10,11]. The values for both ϕ_c and T_c are taken according to the results of Ref. [11]; yet, as already noted by those authors, a clear-cut choice of critical volume fraction is difficult due to the broad, flat maxima of binodal lines. Also, since our experimental data span a range of concentration which is not so close to the critical point, and due to the difficulty in determining the critical point, we believe that the observed value for β is not definitive, and could be improved by further experiments.

B. Limit of stability: Spinodal points

The condition for equilibrium stability in solutions is satisfied if [42]:

$$\left(\frac{\partial \mu}{\partial n} \right)_{T,P} \geq 0, \quad (2)$$

where μ is the solute chemical potential and n is the molar

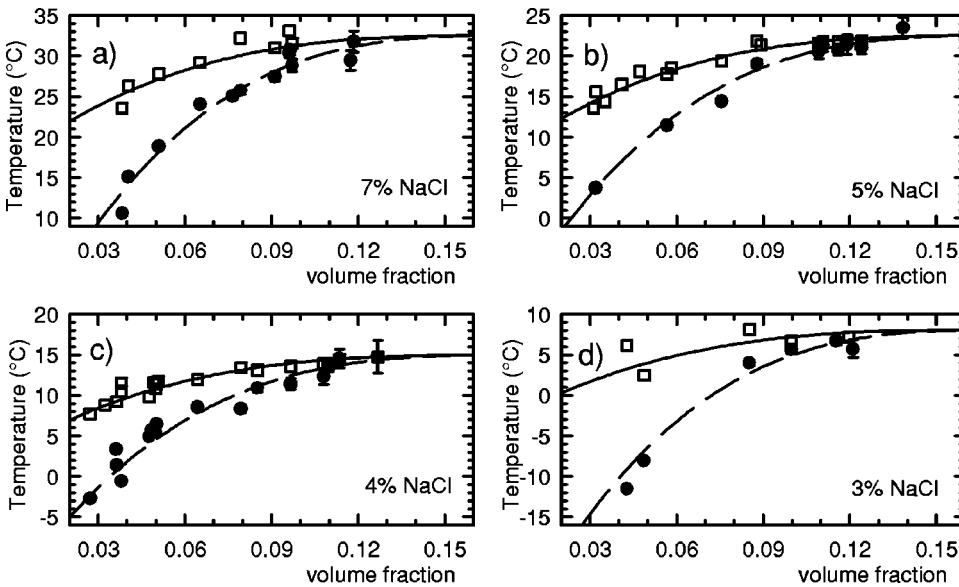


FIG. 2. Phase diagrams at different NaCl concentrations: (a) 7% , (b) 5% , (c) 4% , and (d) 3% w/v. Cloud-point (open squares) and spinodal (circles) experimental data. Solid and dashed lines reproduce, respectively, binodal and spinodal curves as in Eq. (1), with $\beta = 0.325$.

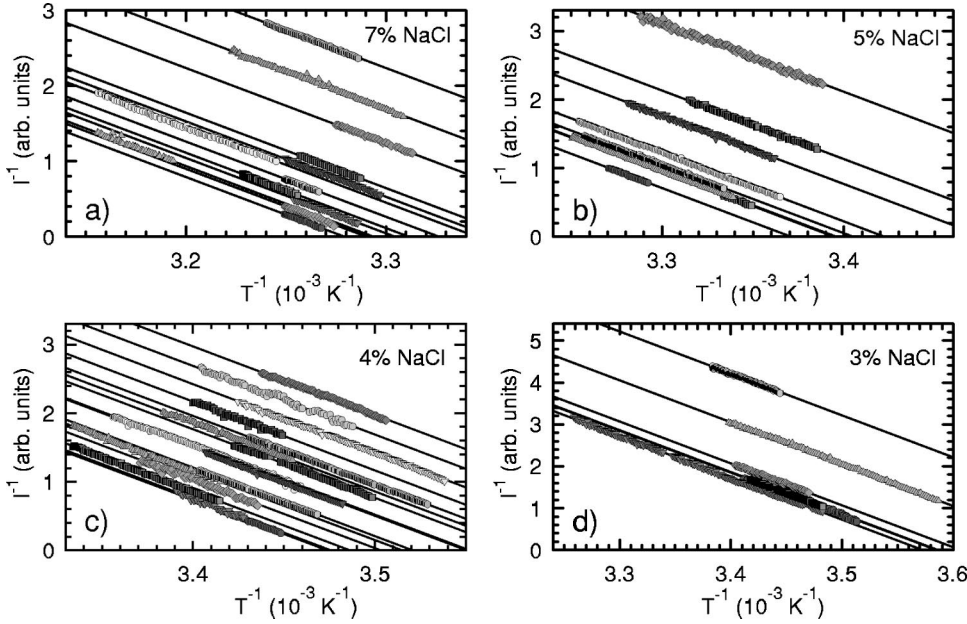


FIG. 3. Divergences of scattered intensity at different protein and salt concentrations. Solid lines are linear fits to data. (a) NaCl 7% w/v; protein volume fractions (from up to down): $\phi = 0.039, 0.040, 0.051, 0.065, 0.076, 0.079, 0.091, 0.097, 0.118, 0.096, 0.097$, and 0.119 . (b) NaCl 5% w/v; $\phi = 0.032, 0.056, 0.075, 0.087, 0.109, 0.110, 0.119$, and 0.138 . (c) NaCl 4% w/v; $\phi = 0.027, 0.038, 0.036, 0.036, 0.048, 0.049, 0.050, 0.079, 0.064, 0.085, 0.097, 0.108, 0.109, 0.113$, and 0.127 . (d) NaCl 3% w/v. $\phi = 0.042, 0.049, 0.085, 0.99$, 0.126 , and 0.115 .

fraction. The boundary of thermodynamic stability, or spinodal line, is defined by the equality in Eq. (2) or equivalently,

$$V \left(\frac{\partial P}{\partial V} \right)_T = k_T^{-1} = 0, \quad (3)$$

where k_T is the isothermal compressibility relative to osmotic pressure P .

Starting from the region of thermodynamic stability, the spinodal line is not experimentally accessible since it is hidden below the coexistence line, except at the critical point, where the system undergoes a second-order phase transition. By approaching the critical point, several thermodynamic quantities exhibit a power law divergence [43]; in particular, the isothermal compressibility diverges with a critical exponent γ . It is evident from Eq. (3) that compressibility diverges at each point on the spinodal line, yet from the theory of phase transitions it is difficult to predict whether the same scaling behavior applies off the critical point.

It has been proposed that the scaling behavior shown by a thermodynamic quantity along the critical isochore can be extended to any isochore with respect to the spinodal temperature $T_{sp}(\phi)$ (pseudospinodal hypothesis) [38]. For example, for the isothermal compressibility

$$k_T = k_0 \left| \frac{T - T_{sp}(\phi)}{T_{sp}(\phi)} \right|^{-\gamma}, \quad (4)$$

where k_0 is a constant amplitude and γ is the critical exponent [39]. This equation provides an experimental method to obtain the spinodal temperature by extrapolating the divergent behavior of a thermodynamic quantity measured in the region of stability. It has been pointed out that the existence of a pseudospinodal line characterized by non-mean-field exponents would imply a singularity in the equation of state in the near-critical region [45–47]. Thus, the concept of the pseudospinodal deserves more study, also in order to clarify if it actually coincides with the limit of stability [39]. This

notwithstanding, the method has been successfully applied to various liquid systems, from binary mixture [45,48] to protein [3,13,14] and other biopolymeric solutions [49].

Isothermal compressibility can be easily determined by light scattering experiments [41]. It is proportional to the structure function $S(q)$ at zero scattering vector $q=0$:

$$\frac{k_T}{k_T^0} = S(0), \quad k_T^0 = \frac{1}{\rho k_B T}, \quad (5)$$

where k_T^0 is the ideal gas compressibility, ρ is the number concentration, and k_B is the Boltzmann constant. On the other hand, the structure function is determined from the following scattered intensity $I(q)$ for objects whose size is much smaller than the wavelength of incident light:

$$I(q) = S(q) I_0 H, \quad (6)$$

where I_0 is a constant related to experimental conditions and $H = [2\pi\tilde{n}(d\tilde{n}/dc)\lambda_0^{-2}]^2 N_A^{-1} c M$ with molar mass M , mass concentration c , medium refractive index \tilde{n} , incident wavelength λ_0 , and Avogadro's number N_A .

The relation between the divergence of scattered intensity and the spinodal temperature results from Eqs. (4)–(6). In particular, when the critical exponent has a mean-field value ($\gamma=1$), one obtains the following expression, which allows for a straightforward extrapolation of inverse intensity:

$$\frac{\text{const.}}{I(0)} = \frac{1}{T_{sp}(\phi)} - \frac{1}{T}. \quad (7)$$

In our experiments we actually found $\gamma=1$. In Fig. 3 data are plotted as in Eq. (7), and the spinodal temperature is calculated by linear fitting. The obtained spinodal points are plotted in Fig. 2.

Extrapolation of the scattered intensity to zero angle could be tricky in many cases, especially near the critical point.

However, in a wide range of temperature above the critical point, the classic Ornstein-Zernike (OZ) expression holds [43]:

$$S(q) = \frac{S(0)}{[1 + (q\xi)^2]^{1-\eta/2}}. \quad (8)$$

Here ξ is the correlation length of concentration fluctuations and η is the critical exponent introduced by Fisher to take into account deviations from mean-field OZ theory ($\eta=0$) [50]. In our experiments we have measured both the 90° scattered intensity (with $q=0.023 \text{ nm}^{-1}$) and the correlation length which is calculated from the correlation function (as will be made clear in the following section). Since experiments were never brought too close to the spinodal temperature, the values of correlation length never exceeded a few tens of nanometer, so that in most cases $q\xi < 1$. Thus, the correction due to the OZ factor introduces only a slight correction in the extrapolation procedure. The difference in the spinodal temperatures, obtained either by using the OZ factor or by ignoring it, was taken as an error estimate and is reported as such in Fig. 2 (when larger than point size).

IV. DIVERGENCE OF CONCENTRATION FLUCTUATIONS

The observed increase and divergence of compressibility, on approaching the spinodal line, is accompanied by an increase in the correlation time τ , measured by dynamic light scattering (Fig. 1). This correlation time, as already recalled in Sec. II, is related to diffusional relaxation of concentration fluctuation through an effective diffusion coefficient $D = \lim_{q \rightarrow 0} (\tau q^2)^{-1}$ [41]. The relation between the correlation length of concentration fluctuations ξ and diffusion coefficient D is given by simple hydrodynamic predictions as well as by a zeroth order mode-mode coupling approach [43,51], and it is formally equivalent to the classic Stokes-Einstein law for a Brownian solute of radius ξ :

$$D = \frac{k_B T}{6\pi\eta_0\xi}, \quad (9)$$

where η_0 is the bulk viscosity.

From the pseudospinodal hypothesis, it follows that the correlation length should diverge critically with a critical exponent ν while approaching the spinodal temperature;

$$\xi = \xi_0 \left| \frac{T - T_{sp}(\phi)}{T_{sp}(\phi)} \right|^{-\nu}. \quad (10)$$

Diffusion coefficients obtained from dynamic light scattering experiments have been fit by using Eqs. (9) and (10) for each salt and protein concentration. In the first run ξ_0 , T_{sp} , and ν were left as free parameters. Best-fit values for the critical exponent ν were all spread within the range 0.60–0.66, with a strong preference of value 0.63 (as in Ref. [4]). Therefore, the fitting procedure was repeated by keeping ν constant and equal to the found average value $\nu = 0.63$. The values of parameter ξ_0 are of the order of molecular size $\xi_0 = 1.0 \pm 0.2 \text{ nm}$, with a slight increasing trend

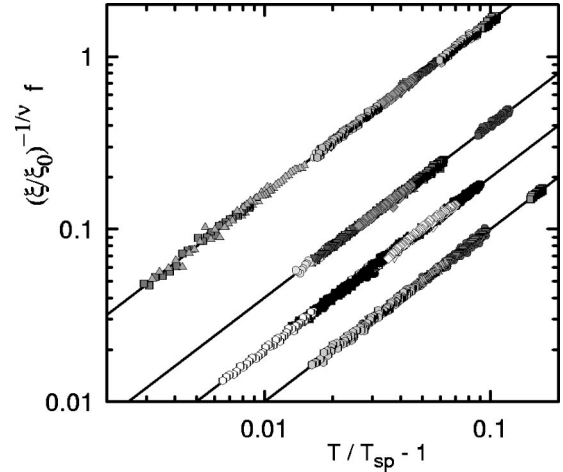


FIG. 4. Scaling of correlation lengths (ξ) at different salt and protein concentrations ($\nu=0.63$). NaCl concentration (from up to down): 7%, 5%, 4%, and 3% w/v. Factor $f = 2^{c_s - 3}$, where c_s is salt concentration in % w/v, has been used to visually separate each salt concentration. Protein concentrations are the same as reported in Fig. 3.

towards higher concentrations, and the values of spinodal temperatures are in acceptable agreement with those found by the compressibility extrapolation (Fig. 3); the differences between the two calculated spinodal sets are taken as a more appropriate error estimate, and reported as such for subsequent analyses (Sec. V).

By using fitting parameters, data have been rescaled into the master curve shown in Fig. 4. The striking scaling of correlation lengths seems to be a robust signature of the critical dynamic behavior of these protein solutions on approaching the limit of stability.

A question arises from a comparison with results shown in the preceding section (on static light scattering data), where the critical exponent γ has a mean-field value ($\gamma = 1$). This can actually be expected, since the temperature range in our experiments stays well above the spinodal line, and far from the critical point. Nevertheless, the other critical exponent ν has a value which is consistent with renormalization-group calculation ($\nu=0.63$) while in mean-field approximation it would be $\nu=0.5$ [44]. Values of the exponents γ and ν would be fully consistent by assuming a value for exponent η , which appears in Eq. (8), of about 0.41, in order to satisfy Fisher equality $\gamma = \nu(2 - \eta)$ [50]. The value of η is very difficult to measure if correlation length ξ is not sufficiently large, that is, if the experiments are not driven very close to spinodal temperature or to the critical point. However, the typical experimental values reported in literature for η are, at least, an order of magnitude lower than 0.41.

We tried to deal with this question by considering a less severe approximation in the context of mode-mode coupling approach, by including a background and a critical term in the correlation length expression [51,52]. We report in the Appendix such results.

An attempt to rationalize this non-mean-field behavior can be issued by the following qualitative argument that

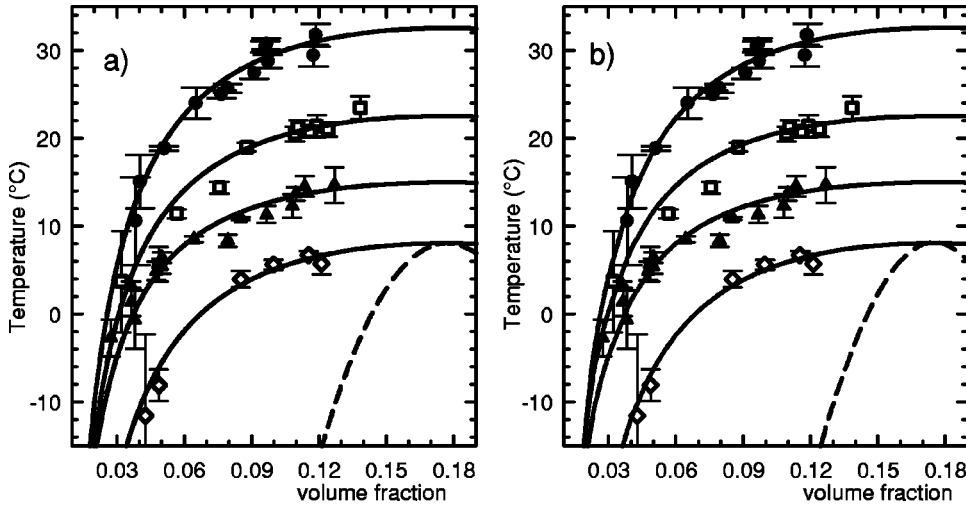


FIG. 5. Fitting of spinodal points. Experimental data: NaCl 7% w/v (circles), 5% w/v (squares), 4% w/v (triangles), and 3% w/v (diamonds). Solid lines are spinodal predictions obtained as described in the text for two reference models: (a) van der Waals [Eqs. (12) and (13)], and (b) Adhesive Hard-Spheres [Eqs. (14), (17), (18), and (21)]. Dashed lines are spinodal curves with a zero perturbative entropy.

would need a more solid theoretical foundation. Mean-field behavior of a diverging thermodynamic quantity is related to the difference between the experimental temperature T and the critical temperature T_{sp} . The crossover from mean-field to fluctuation dominated behavior in the context of Ginzburg-Landau theory of phase transition is stated by the Ginzburg criterion which indicates at what reduced temperature $t_G = |T - T_c|/T_c$ the breakdown of the Gaussian (mean-field) approximation occurs [44]. Moreover, the crossover is not necessarily the same for all thermodynamic quantities. The crossover temperature is roughly given by $t_G \sim (u_4/\lambda)^6$ [53], where u_4 is the first nonGaussian term in Landau-Ginzburg free energy in units of $[k_B T]$ and λ is the ratio between the range of interaction and the molecular size. The term u_4 is typically of order unity, thus crossover is mainly due to the relative range of molecular interactions $t_G \sim \lambda^{-6}$. Thus, we could argue that the correlation function of critical fluctuations and the related correlation length are mainly sensitive to solution structure as determined by short-range interactions [$\lambda \sim O(1)$]. Thus, our experimental temperatures would be fully within the Ginzburg region, and we would correctly observe a non-mean-field value for ν . On the other hand, compressibility is probably sensitive to more long-range (bulk) properties of solution, since it is related to the structure function in the hydrodynamic limit $q=0$. Therefore, it could be acceptable to observe a mean-field scaling behavior even very close to critical temperature.

V. MODELING MOLECULAR INTERACTIONS

Knowledge of the spinodal line offers a great advantage in determining protein-protein interactions in solutions. Indeed, an analytic expression for the spinodal line can be derived from the equation of state or from the density correlation function, or from any thermodynamic quantity which allows calculating an expression for the isothermal compressibility k_T [Eqs. (3)–(5)].

A simple equation of state, that actually owes an enduring success to its capability of describing liquid-vapor equilibria, is the classical van der Waals equation. This is a mean-field equation which takes into account, approximately, both ex-

cluded volume effects and effects of attractive intermolecular forces; it can be used to represent solute-solute “mean-force” interactions in solution after averaging over the solvent degrees of freedom. The van der Waals model yields the following expressions for pressure P and the $q=0$ structure function $S(0)$ of a system of particles of volume v_s [39]:

$$v_s \beta P = \frac{\phi}{1 - b\phi} - \beta a \phi^2, \quad (11)$$

$$S(0)^{-1} = \frac{1}{(1 - b\phi)^2} - 2\beta a \phi, \quad (12)$$

where $\beta = (k_B T)^{-1}$. The positive constants a and b are related to the critical volume fraction and temperature, $\phi_c = (3b)^{-1}$, and $T_c = (8/9)\phi_c a/k_B$.

Expression (12) was not sufficient to correctly account for the shape of our experimental spinodals, thus we tried to generalize the model. Here, we have modified the van der Waals equation in an analogy to what has been proposed for polymer solutions [54]. Indeed, constant a (whose dimensions are energy per particle per unit volume fraction) represents a mean-field interaction and thus it is, essentially, related to a free energy more than to an actual energy, since it implies an average over many degrees of freedom. Hence, parameter a can be reasonably modified by including both an energetic (or enthalpic) and an entropic term [55],

$$a = h - Ts. \quad (13)$$

The critical volume fraction is not changed by this generalization, while the critical temperature becomes $T_c = g(8/9)\phi_c(h/k_B)$, where $g = [1 + (8/9)\phi_c s/k_B]^{-1}$.

Spinodal lines can be calculated by equating to zero $S(0)^{-1}$ in Eq. (12). In Fig. 5(a) such curves fit our experimental data. As in Fig. 2, the same critical volume fraction has been used $\phi_c = 0.177$ and $T_c = 32.5, 22.5, 15.0,$ and 8.1°C respectively for $[\text{NaCl}] = 7\%, 5\%, 4\%,$ and 3% w/v. The other parameters are listed in Table I.

This generalized van der Waals model seems able to capture some main features that explain the liquid-liquid phase

TABLE I. Fitting parameters for spinodal lines in Fig. 5: van der Waals (vdw) [Eqs. (12) and (13)] and Adhesive Hard-Sphere (AHS) [Eqs. (14), (17), (18), and (21)] model.

c_s	b	vdW		Θ^c	u ^a	AHS ($\lambda = 1.05$)		Θ^c
		h^a	s^b			h^a	s^b	
7%	1.88	75 ± 15	0.24 ± 0.05	44	0.20	74 ± 1	0.23 ± 0.03	39
5%	1.88	85 ± 30	0.27 ± 0.10	32	0.20	90 ± 1	0.29 ± 0.04	27
4%	1.88	95 ± 40	0.32 ± 0.10	23	0.20	96 ± 1	0.32 ± 0.04	19
3%	1.88	60 ± 20	0.22 ± 0.08	19	0.02	60 ± 1	0.20 ± 0.04	16

^a[Kcal/mol/K].

^b[Kcal/mol].

^c[°C] At Θ temperature $B_2 = 0$.

transition in our protein solutions, though it is not able to represent the liquid-solid coexistence, which is the actual equilibrium state in these systems. Indeed, in the van der Waals model, repulsive interactions are treated in a very simplified way.

An alternative approach, based on standard perturbation theories, can be used to describe equations of state and phase equilibria in simple liquids [56]. In this approach, weak or long-range interactions are treated perturbatively with respect to a reference potential which typically includes excluded volume effects and short-range attraction, and is considered explicitly in all calculations. Equations for pressure P and structure function at zero q vector $S(0)$ read

$$v_s \beta P = v_s \beta P_0 - \beta a \phi, \quad (14)$$

$$S(0)^{-1} = S_0(0)^{-1} - 2\beta a \phi, \quad (15)$$

where, subscript 0 denotes the reference quantities, $v_s = \sigma^3 \pi/6$ is the solute volume, ϕ is the volume fraction, and $\beta = (k_B T)^{-1}$. If one deals with a long-range potential $w(\vec{r})$ representing the interaction between two particles at distance $|\vec{r}|$ then, in the Random Phase Approximation, parameter a (corresponding to the van der Waals attraction term) represents the perturbation energy density per unit volume fraction and is given by $a = (2v_s)^{-1} \int w(\vec{r}) d\vec{r}$ [56].

As to the reference potential, the easier choice is to model the system as hard spheres, neglecting other types of attraction [6]. For such a system, explicit expressions for both pressure and compressibility have been derived, via the Percus-Yevick approximation [56] or the Carnahan-Starling formula [57]. However, both these approximations yield a critical volume fraction which is around 0.13 and thus they oddly reproduce previous and present results on lysozyme solutions [3,7,10,11].

In the last decade, the existence of a liquid-liquid phase transition, metastable with respect to solid-liquid coexistence in protein or colloidal solutions, has been explained by modeling solute interactions through a short-range attractive potential [15,16,18,19,21]. There is also a growing experimental evidence that short-range interactions are important in determining some properties of such solutions, especially at low concentrations and high ionic strength [58–60], even if

long-range forces (van der Waals attraction, electrostatic repulsion, etc.) also contribute in determining the phase diagram [61–63].

Here we consider the case of a square-well potential for a spherical particle with a hard core of diameter σ and a range of interaction $\lambda \sigma$ given as

$$v_{sw}(r) = \begin{cases} \infty, & r < \sigma \\ -u, & \sigma \leq r \leq \lambda \sigma \\ 0, & \lambda \sigma < r. \end{cases} \quad (16)$$

In the limit of an infinitely narrow and deep well (Adhesive Hard Spheres) Baxter derived, in the Percus-Yevick approximation, an explicit expression for compressibility [64]:

$$S_0(0)^{-1} = \frac{(1 + 2\phi - \mu)^2}{(1 - \phi)^4}, \quad (17)$$

where

$$\mu = \frac{b - \sqrt{b^2 - 12\phi - 6\phi^2}}{\phi(1 - \phi)}, \quad b = 6\tau(1 - \phi) + 6\phi \quad (18)$$

and

$$\tau^{-1} = \lim_{\substack{\lambda \rightarrow 1 \\ u \rightarrow \infty}} 12 \frac{\lambda - 1}{\lambda} e^{\beta u}. \quad (19)$$

The so-called stickiness parameter τ indicates deviation of the second virial coefficient B_2 from that of hard spheres:

$$\frac{B_2}{B_2^{HS}} = 1 - \frac{1}{4\tau}. \quad (20)$$

The same expression for compressibility holds for a square-well potential to zero order in $(1 - \lambda^{-1})$ [65], with the following mapping of stickiness into square-well parameters:

$$\tau^{-1} = 4(\lambda^3 - 1)(e^{\beta u} - 1). \quad (21)$$

We used adhesive hard spheres as a reference system and Eqs. (14), (17), (18), and (21) to fit our spinodal data, as shown in Fig. 5(b). The value of λ has been fixed to 1.05

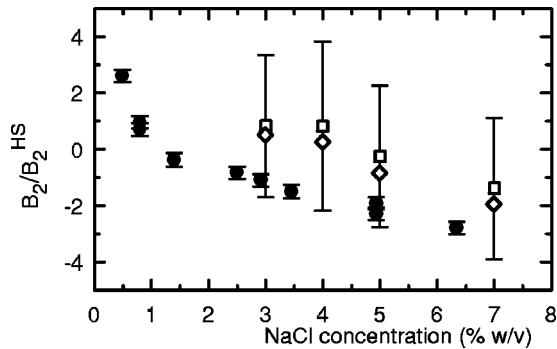


FIG. 6. Second virial coefficients vs salt concentration. Squares and diamonds are calculated from parameters of spinodal lines in Fig. 5(a) and Fig. 5(b), respectively. Circles are experimental data taken from Ref. [19].

(which is reasonable for lysozyme in such conditions). The value of potential u is critical to determine the position of the critical volume fraction, and it has been fixed in order to obtain $\phi_c = 0.177$. Fitting parameters are listed in Table I.

As evident from Table I, both the van der Waals and the Adhesive Hard-Sphere models give comparable fitting to experimental data, with comparable parameter of the perturbative (long range?) attractive part. What is relevant in both cases is the presence of the entropic term s . In Fig. 5 a typical curve with $s = 0$ has been reported for reference. It seems that this entropic contribution is essential to reproduce the correct width of experimental spinodal lines. Interestingly, both models yield comparable values of second virial coefficients, as shown in Fig. 6 for a reference temperature (25°C), and in Table I, where the Θ temperature has been reported, which is the temperature at which the solution has an ideal behavior ($B_2 = 0$). In Fig. 6 experimental points for the direct measurement of the second virial coefficient are also reproduced from Ref. [19]. The comparison is noteworthy if one considers that our B_2 data are derived through a quite indirect route. In fact, our calculated B_2 are all above experimental values, yet salt concentration dependence is well reproduced. We take this rough agreement as a further indication that our model is able to capture some basic features of the interactions involved.

From inspection of Table I, it also results that the effect of salt is in a subtle balance between the enthalpic and the entropic term. These terms have a non-monotonic dependence upon salt concentrations. This interesting behavior is not unexpected, since it matches analogous results on lysozyme solutions [10,12]. As to a recent simulation work, such non-monotonic behavior could be ascribed to the nonuniform distribution of charges on protein surface, and the corresponding nonuniform distribution of counterions [66]. A more detailed physical explanation of this behavior can hardly be extracted from our data which actually claims for a more extensive study of this effect.

The model of hard spheres with short-range attraction, which sounds appropriate for colloids in solutions, could probably be improved for globular proteins, since they have a complex shape and a highly structured surface. Other model interactions have been proposed to incorporate highly

directional interactions (sticky patches [67], or aeolotropic interactions [68–70]). Our results clearly suggest the need for further modeling efforts to rationalize the width of the instability region, that is, in our approach, to account for an “entropic” term of type $TS\phi^2$ in the free energy per particle of the system. For example, Warren has recently proposed an interesting model which supplies an additive “entropic” term to compressibility by taking into account the mixing free energy of ions and counterions in salted solutions of charged proteins [71]; yet, at our salt concentrations this contribution is too weak to account for the correct width of spinodal line. In particular, a main ingredient, probably missing in current theories, is the explicit role of solvent, which we have implicitly considered in mean-field approximation. Hydrophobicity and hydration are complex, nonadditive effects in biological molecules and it is a subtle matter to average them out [72].

VI. CONCLUSIONS

In the present work, we have measured, by static and dynamic light scattering experiments, the amplitude of concentration fluctuations and their correlation length, in solution of lysozyme at $\text{pH } 4.5$ and at different ionic strength (NaCl concentrations of 3%, 4%, 5%, and 7% w/v). Under such conditions, and for a wide range of temperatures and concentrations, the equilibrium state is the coexistence between solid and liquid phases [2]. In supersaturated solutions, in which the crystal nucleation has not yet started, the solution is known to have a liquid-liquid phase transition that affects the initial kinetics of crystal growth, and determines solution properties [3,7,10–12].

We found that both the amplitude and correlation length of fluctuations show a clear divergent behavior by approaching a given critical temperature. By extrapolating the critical divergent behavior we have determined the limit of stability, that is, the spinodal line. This procedure is grounded on the (pseudospinodal) hypothesis that thermodynamic quantities exhibit, with respect to spinodal points, the same scaling critical behavior that they show with respect to the critical point [38]. This hypothesis has been given here strong experimental support for the case of protein solution.

Cloud-point measurements were also used to determine liquid-liquid coexistence phase boundary, consistent with previous work [11].

A mean-field exponent $\gamma = 1$ has been found for the divergence of the amplitude of concentration fluctuations, related to k_T . The correlation length of concentration fluctuations has been measured over a large range of concentrations off the critical point. It has been shown that correlation length exhibits the same scaling behavior towards spinodal temperatures with a nonclassical exponent $\nu = 0.63 \pm 0.03$.

The interesting discrepancy between a classical compressibility exponent γ and a nonclassical correlation length exponent ν has been discussed. At first, a classical exponent would be expected, since experiments cannot be performed too close to the spinodal temperatures due to the metastable liquid-liquid demixing and the eventual crystal nucleation. Thus, we considered higher order hydrodynamic corrections

(obtained in mode-mode coupling theory) so as to include a background and a critical term in the correlation length expression [51,52] (see Appendix). Within experimental errors, neither approach can be ruled out even if the scaling with $\nu=0.63$ has a much higher quality.

It has been shown that fluctuations close to the critical point may be relevant in enhancing crystal nucleation [34] due to their growing amplitude. Our experiments show that off-critical fluctuations also exhibit divergent scaling behavior, and thus they may have a role in the crystallization process that is yet to be worked out.

We have interpreted our experimental results by modeling protein interactions in solution. Two models have been used: a generalized van der Waals model, and the Adhesive Hard-Spheres model with perturbative long-range attraction. The different roles of steric repulsion, short- and long-range attractions has been extensively studied in literature [73]. What emerges from our results is the existence of a perturbative entropic term that must be taken into account to appropriately reproduce the width of the region of thermodynamic instability. We think that this contribution could be due to the role of hydration water.

Our analysis explains the effect of salt in raising the temperature of the thermodynamic instability and in causing protein salting-out as due to a subtle balance between enthalpic and entropic contributions to the free energy of protein-solvent mixing, consistent with the quasiphenomenological picture of salt competing with water for the hydration of protein.

As a concluding remark, we note that our results enhance our understanding of phase diagrams of protein solutions and of the role of fluctuations and salts, but they also prompt several intriguing questions to be addressed, both experimentally and theoretically.

ACKNOWLEDGMENTS

The first part of this work was initiated at the Department of Physics of the University of Palermo, and inspired by Professor M. U. Palma, who is here acknowledged. We thank Professor F. Sciortino for useful discussions, Dr. D. Giacomazza for support in the rheological measurements, and Professor J. Newman for critical reading of the manuscript. One of the authors (C.X.) acknowledges partial financial support from the Italian Institute for Condensed Matter Physics (INFM).

APPENDIX: MODE-COUPLING APPROACH TO CONCENTRATION FLUCTUATIONS

Here, we try to address the discrepancy between the mean-field value of exponent γ and the nonclassical value of exponent ν by relaxing the hypothesis taken by applying Eq. (9). A correction to hydrodynamics predictions was introduced by Botch and Fixman [45,74] by modifying the diffusion coefficient in Eq. (9) with terms of higher order in q^2 ; the first-order correction leads to a OZ-like factor $[1 + (\xi q)^2]$. As already noted in the preceding section, this correction is irrelevant in our experiments since ξq is small.

Moreover, it would not help in lowering the value of the exponent towards the mean-field value. A correction that could be, in principle, more relevant is predicted by mode-mode coupling theory by considering that the diffusion coefficient, as well as other slowly varying transport coefficients (e.g., viscosity), result from the sum of a critical and a background contribution $D = D_c + D_0$ [48,51,75]. In the OZ approximation the background and the critical contributions to the diffusion coefficient are respectively, [52,76]:

$$D_b = \frac{k_B T}{6 \pi \eta_0 \xi} \frac{1 + \xi^2 q^2}{\xi q_c}, \quad D_c = \frac{k_B T}{6 \pi \eta \xi} \frac{(1 + \xi^2 q^2)^z}{K_0(\xi q)^{z-1}}, \quad (\text{A1})$$

where $q_c^{-1} = \xi_c = [6 \pi \eta_0 \xi_0 / (k_B T)] \alpha_0 k_0^{-1} \xi_0$, α_0 and η_0 are, respectively, the background concentration conductivity and the background viscosity, ξ_0 and k_0 , respectively, are the amplitude of diverging correlation length and compressibility [Eqs. (4) and (10)], and $K_0(x) = 0.75x^{-2}[1 + x^2 + (x^3 - x^{-1})\arctan(x)]$ is the Kawasaki function [51]. In addition, viscosity η diverges with the law $\eta = \eta_0(u q_c \xi)^z$, with $u \sim 0.675$ and $z \sim 0.054$ [52].

For $\xi q \ll 1$ Eqs. (A1) can be simplified to the form [75]

$$D = \frac{k_B T}{6 \pi \eta_0 \xi} \left[1 + \frac{\xi_c}{\xi} \right]. \quad (\text{A2})$$

Data were fitted by using the latter equation and Eq. (10), with the critical exponent fixed at the mean-field value $\nu = 0.5$ and the spinodal temperatures taken from best fits of Fig. 3. We found $\xi_0 = 1.5 \pm 0.3$ nm and $\xi_c = 200 \pm 100$ nm. The value of ξ_c is two orders of magnitude higher than molecular size, and it is a quite large value in comparison with what found in binary mixtures [48,75] but comparable with the value found in protein solutions [8]. In order to allow for a comparison with master curves of Fig. 4, we have plotted data (for one salt concentration) so as to clearly show the scaling behavior by using the effective correlation length ξ^* :

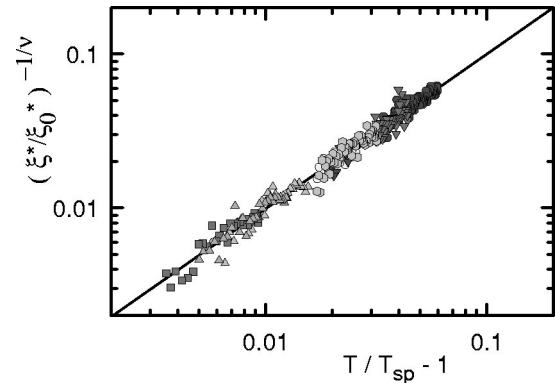


FIG. 7. Scaling of correlation lengths (ξ^*) at NaCl 7% w/v, by taking into account both a critical and a background term ($\nu = 0.5$). Protein concentrations are the same as in Fig. 3 for $\phi > 0.080$.

$$\frac{\xi_0^*}{\xi^*} = \frac{\xi_0}{\xi_c} \left[\frac{6\pi\eta_0 D}{k_B T} \xi_0 \left| \frac{T - T_{sp}}{T_{sp}} \right|^{-0.5} - 1 \right]. \quad (\text{A3})$$

For other salt concentrations considered in this work we obtained scalings of quality comparable to that of Fig. 7.

The scaling behavior observed in this approach has a poorer quality with respect to that observed by assuming a non-mean-field value of the critical exponent ν . Thus, sticking to the experimental facts, we can conclude that our results clearly show the existence of a dynamic scaling behavior in off-critical protein solutions, but a complete theoretical description of this phenomenon is still missing.

-
- [1] J.C. Rochet and P.T.J. Lansbury, *Curr. Opin. Struct. Biol.* **10**, 60 (2000).
- [2] A. McPherson, *Crystallization of Biological Macromolecules* (Cold Spring Harbor Laboratory Press, Cold Spring Harbor, NY, 1999).
- [3] C. Ishimoto and T. Tanaka, *Phys. Rev. Lett.* **39**, 474 (1977).
- [4] P. Schurtenberger, R.A. Chamberlin, G.M. Thurston, J.A. Thomson, and G.B. Benedek, *Phys. Rev. Lett.* **63**, 2064 (1989).
- [5] M.L. Broide, C.R. Berland, J. Pande, and O.O. Ogun, *Proc. Natl. Acad. Sci. U.S.A.* **88**, 5660 (1991).
- [6] C.R. Berland, G.M. Thurston, M. Kondo, M.L. Broide, J. Pande, O.O. Ogun, and G.B. Benedek, *Proc. Natl. Acad. Sci. U.S.A.* **89**, 1214 (1992).
- [7] V.G. Taratuta, A. Holschbach, G.M. Thurston, and D. Blankstein, *J. Phys. Chem.* **94**, 2140 (1990).
- [8] B.M. Fine, J. Pande, A. Lomakin, O.O. Ogun, and G.B. Benedek, *Phys. Rev. Lett.* **74**, 198 (1995).
- [9] B.M. Fine, A. Lomakin, O.O. Ogun, and G.B. Benedek, *J. Chem. Phys.* **104**, 326 (1996).
- [10] M.L. Broide, T.M. Tominc, and M.D. Saxowsky, *Phys. Rev. E* **53**, 6325 (1996).
- [11] M. Mushol and F. Rosenberger, *J. Chem. Phys.* **107**, 1953 (1997).
- [12] J.J. Grigsby, H.V. Blanch, and J.M. Prausnitz, *Biophys. Chem.* **91**, 231 (2001).
- [13] P.L. San Biagio and M.U. Palma, *Biophys. J.* **60**, 508 (1991).
- [14] P.L. San Biagio, D. Bulone, A. Emanuele, and M.U. Palma, *Biophys. J.* **70**, 494 (1996).
- [15] A.P. Gast, W.B. Russel, and C.K. Hall, *J. Colloid Interface Sci.* **96**, 251 (1983).
- [16] H.N.W. Lekkerkerker, W.-C. Poon, P.N. Pusey, A. Stroobants, and P.B. Wariën, *Europhys. Lett.* **20**, 559 (1992).
- [17] S.M. Ilett, A. Orrock, W.C.K. Poon, and P.N. Pusey, *Phys. Rev. E* **51**, 1344 (1995).
- [18] M.H.J. Hagen and D. Frenkel, *J. Chem. Phys.* **101**, 4093 (1994).
- [19] D. Rosenbaum, P.C. Zamora, and C.F. Zukoski, *Phys. Rev. Lett.* **76**, 150 (1996).
- [20] M.G. Noro and D. Frenkel, *J. Chem. Phys.* **113**, 2941 (2000).
- [21] G. Foffi, G.D. McCullagh, A. Lawlor, E. Zaccarelli, K.A. Dawson, F. Sciortino, P. Tartaglia, D. Pini, and G. Stell, *Phys. Rev. E* **65**, 031407 (2002).
- [22] A. George and W.W. Wilson, *Acta Crystallogr.* **50**, 361 (1994).
- [23] R.M.L. Evans, W.C.K. Poon, and M.E. Cates, *Europhys. Lett.* **38**, 595 (1997).
- [24] N.M. Dixit, A.M. Kulkarni, and C.F. Zukoski, *Colloids Surf., A* **190**, 47 (2001).
- [25] J. Drenth and C. Haas, *Acta Crystallogr.* **54**, 867 (1998).
- [26] O. Galkin and P.G. Vekilov, *Proc. Natl. Acad. Sci. U.S.A.* **97**, 6277 (2000).
- [27] R.P. Sear, *Phys. Rev. E* **63**, 066105 (2001).
- [28] W.C.K. Poon, *Phys. Rev. E* **55**, 3762 (1997).
- [29] V. Bhamidi, E. Skrzypczak-Jankun, and C.A. Schall, *J. Cryst. Growth* **232**, 77 (2001).
- [30] Y. Georgalis, P. Umbach, D.M. Soumpasis, and W. Saenger, *J. Am. Chem. Soc.* **120**, 5539 (1998).
- [31] S. Tanaka, M. Ataka, and K. Ito, *Phys. Rev. E* **65**, 051804 (2002).
- [32] D.N. Petsev and P.G. Vekilov, *Phys. Rev. Lett.* **84**, 1339 (2000).
- [33] W.J.K. Poon, S.U. Egelhaaf, P.A. Beales, A. Salonen, and L. Sawyer, *J. Phys.: Condens. Matter* **12**, 569 (2000).
- [34] P.R. ten Wolde and D. Frenkel, *Science* **277**, 1975 (1997).
- [35] Y.C. Shen and D.W. Oxtoby, *J. Chem. Phys.* **104**, 4233 (1996).
- [36] V. Talanquer and D.W. Oxtoby, *J. Chem. Phys.* **109**, 223 (1998).
- [37] S.M. Vaiana, M.B. Palma-Vittorelli, and M.U. Palma, *Proteins* **51**, 147 (2003).
- [38] G.B. Benedek, in *Polarisation, Matière et Rayonnement; Volume Jubilaire en l'Honneur d'Alfred Kastler* (Presses Universitaires de France, Paris, 1969).
- [39] P.G. Debenedetti, *Metastable Liquids: Concepts and Principles* (Princeton University Press, Princeton, NJ, 1996).
- [40] A.J. Sophianopoulos, C.K. Rhodes, D.N. Holcomb, and K.E. Van Holde, *J. Biol. Chem.* **237**, 1107 (1962).
- [41] B.J. Berne and R. Pecora, *Dynamic Light Scattering* (Wiley Interscience, New York, 1976).
- [42] J.G. Kirkwood and I. Oppenheim, *Chemical Thermodynamics* (McGraw-Hill, New York, 1961).
- [43] H.E. Stanley, *Introduction to Phase Transition and Critical Phenomena* (Oxford University Press, New York, 1971).
- [44] D.J. Amit, *Field Theory, the Renormalization Group, and Critical Phenomena* (World Scientific, Singapore, 1984).
- [45] B. Chu, F.J. Schoenes, and M.E. Fisher, *Phys. Rev.* **185**, 219 (1969).
- [46] C.M. Sorensen and M.D. Semon, *Phys. Rev. A* **21**, 340 (1980).
- [47] C.M. Sorensen, *J. Chem. Phys.* **94**, 8330 (1991).
- [48] S.H. Chen, C.C. Lai, J. Rouch, and P. Tartaglia, *Phys. Rev. A* **27**, 1086 (1983).
- [49] M. Manno, A. Emanuele, V. Martorana, P.L. San Biagio, D. Bulone, M.B. Palma-Vittorelli, D.T. McPherson, J. Xu, T.M. Parker, and D.W. Urry, *Biopolymers* **59**, 51 (2001).
- [50] M.E. Fisher, *J. Math. Phys.* **5**, 944 (1964).
- [51] K. Kawasaki, *Ann. Phys.* **61**, 1 (1970).

- [52] D.W. Oxtoby and W.M. Gelbart, *J. Chem. Phys.* **61**, 2957 (1974).
- [53] M.E. Fisher, *Phys. Rev. Lett.* **57**, 1911 (1986).
- [54] P.J. Flory, *Principles of Polymer Chemistry* (Cornell University Press, Ithaca, 1953).
- [55] J.W. Jansen, C.G. De Kruif, and A. Vrij, *Chem. Phys. Lett.* **107**, 450 (1984).
- [56] J.P. Hansen and I.R. McDonald, *Theory of Simple Liquids* (Academic Press, London, 1986).
- [57] N.F. Carnahan and K.E. Starling, *J. Chem. Phys.* **51**, 635 (1969).
- [58] A. Kulkarni and C.F. Zukoski, *J. Cryst. Growth* **232**, 156 (2001).
- [59] R. Piazza, V. Peyre, and V. Degiorgio, *Phys. Rev. E* **58**, R2733 (1998).
- [60] M. Malfois, F. Bonnet, A. Tardieu, and L. Belloni, *J. Chem. Phys.* **105**, 3290 (1996).
- [61] M.G. Noro, N. Kern, and D. Frenkel, *Europhys. Lett.* **48**, 332 (1999).
- [62] R.P. Sear, *Phys. Rev. E* **61**, 6019 (2000).
- [63] G. Pellicane, D. Costa, and C. Caccamo, *J. Phys.: Condens. Matter* **15**, 375 (2003).
- [64] R.J. Baxter, *J. Chem. Phys.* **49**, 2770 (1968).
- [65] W.R. Chen, S.H. Chen, and F. Mallamace, *Phys. Rev. E* **66**, 021403 (2002).
- [66] E. Allahyarov, H. Lowen, J.P. Hansen, and A.A. Louis, *Phys. Rev. E* **67**, 051404 (2003).
- [67] R.P. Sear, *J. Chem. Phys.* **111**, 4800 (1999).
- [68] N. Asherie, A. Lomakin, and G.B. Benedek, *Phys. Rev. Lett.* **77**, 4832 (1996).
- [69] A. Lomakin, N. Asherie, and G.B. Benedek, *J. Chem. Phys.* **104**, 1646 (1996).
- [70] A. Lomakin, N. Asherie, and G.B. Benedek, *Proc. Natl. Acad. Sci. U.S.A.* **96**, 9465 (1999).
- [71] P.B. Warren, *J. Phys.: Condens. Matter* **14**, 7617 (2002).
- [72] D. Bulone, V. Martorana, P.L. San Biagio, and M.B. Palma-Vittorelli, *Phys. Rev. E* **62**, 6799 (2000).
- [73] R. Piazza, *Curr. Opin. Colloid Interface Sci.* **5**, 38 (2000).
- [74] W. Botch and M. Fixman, *J. Chem. Phys.* **42**, 199 (1965).
- [75] C.M. Sorensen, *J. Phys. Chem.* **92**, 2367 (1988).
- [76] H.C. Burstyn and J.V. Sengers, *Phys. Rev. A* **25**, 448 (1982).